The Laryngoscope

Hybrid Three-Dimensional–Printed Ear Tissue Scaffold With Autologous Cartilage Mitigates Soft Tissue Complications

Brian Chang, MD, MS[#]; Ashley Cornett, MS[#]; Zahra Nourmohammadi, PhD; Jadan Law; Blaine Weld; Sarah J. Crotts, MS; Scott J. Hollister, PhD; Isabelle M. A. Lombaert, PhD, MS; David A. Zopf, MD, MS

Objectives/Hypothesis: To analyze the use of highly translatable three-dimensional (3D)–printed auricular scaffolds with and without novel cartilage tissue inserts in a rodent model.

Study Design: Preclinical rodent animal model.

Methods: This prospective study assessed a single-stage 3D-printed auricular bioscaffold with or without porcine cartilage tissue inserts in an athymic rodent model. Digital Imaging and Communications in Medicine computed tomography images of a human auricle were segmented to create an external anatomic envelope filled with orthogonally interconnected spherical pores. Scaffolds with and without tissue inset sites were 3D printed by laser sintering bioresorbable polycaprolactone, then implanted subcutaneously in five rats for each group.

Results: Ten athymic rats were studied to a goal of 24 weeks postoperatively. Precise anatomic similarity and scaffold integrity were maintained in both scaffold conditions throughout experimentation with grossly visible tissue ingrowth and angiogenesis upon explantation. Cartilage-seeded scaffolds had relatively lower rates of nonsurgical site complications compared to unseeded scaffolds with relatively increased surgical site ulceration, though neither met statistical significance. Histology revealed robust soft tissue infiltration and vascularization in both seeded and unseeded scaffolds, and demonstrated impressive maintenance of viable cartilage in cartilage-seeded scaffolds. Radiology confirmed soft tissue infiltration in all scaffolds, and biomechanical modeling suggested amelioration of stress in scaffolds implanted with cartilage.

Conclusions: A hybrid approach incorporating cartilage insets into 3D-printed bioscaffolds suggests enhanced clinical and histological outcomes. These data demonstrate the potential to integrate point-of-care tissue engineering techniques into 3D printing to generate alternatives to current reconstructive surgery techniques and avoid the demands of traditional tissue engineering.

Key Words: Three-dimensional printing, auricular reconstruction, tissue engineering.

Level of Evidence: NA

***Laryngoscope*, 131:1008–1015, 2021**

From the Department of Pediatrics (B.C.), University of California Los Angeles Mattel Children's Hospital, Los Angeles, California, U.S.A.; Department of Biologic and Materials Sciences, School of Dentistry (A.C., I.M.A.L.), University of Michigan, Ann Arbor, Michigan, U.S.A.; Biointerfaces Institute (A.C., I.M.A.L.), University of Michigan, Ann Arbor, Michigan, U.S.A.; Department of Otolaryngology–Head and Neck Surgery (Z.N.), University of Michigan, Ann Arbor, Michigan, U.S.A.; Department of Biomedical Engineering (J.L., B.W., D.A.Z.), Michigan Engineering, Ann and Robert H. Lurie Biomedical Engineering Building, Ann Arbor, Michigan, U.S.A.; Center for 3D Medical Fabrication, Coulter Department of Biomedical Engineering (S.J.C., S.J.H.), Georgia Institute of Technology, Atlanta, Georgia, U.S.A.; and the Department of Otolaryngology–Head and Neck Surgery, Michigan Medicine (D.A.Z.), C.S. Mott Children's Hospital, Ann Arbor, Michigan, U.S.A.

Editor's Note: This Manuscript was accepted for publication on June 30, 2020.

[#]B.C. and A.C. are co–first authors.

Accepted as a podium presentation American Society of Preventive Oncology 2020 in Atlanta, GA, but the conference was cancelled due to the Covid pandemic. The presentation was resubmitted as an ePoster.

B.C. was funded through the MICHR TL1 grant (TL1TR002242) during this work. The University of Michigan SoD mCT core in which microCT was conducted was funded in part by the National Institutes of Health/ National Center for Research Resources (S10RR026475–01).

S.J.H. is a cofounder and shareholder of Tissue Regeneration Systems Inc. S.J.H. and D.A.Z. are coinventors on a patent titled Ear Tissue Implant for Auricular Tissue Reconstruction. D.A.Z. is a founder in the startup MakeMedical, which utilizes the technology listed in this article and was formed to commercialize intellectual property related to three-dimensional printing, but the research was not funded by the company.

The authors have no other funding, financial relationships, or conflicts of interest to disclose.

Send correspondence to David Zopf, MD, MS, Department of Pediatric Otorhinolaryngology–Head and Neck Surgery, C.S. Mott Children's Hospital, Michigan Medicine, 1540 E Hospital Drive, SPC 4241, Ann Arbor, MI 48109-4241. E-mail:davidzop@med.umich.edu

DOI: 10.1002/lary.29114

INTRODUCTION

Auricular reconstruction is a complex and technically challenging endeavor. The most common repair technique involves the creation and implantation of an autologous construct fashioned by hand from costal cartilage, generally yielding acceptable aesthetic outcomes with a durable and compatible implant.[1,2] However, the process is demanding given the intricacy of repair, significant psychosocial sequelae, and potential complications including pneumothorax, infection, exposure of the implant, and scarring. Although porous polyethylene (PPE) implants (e.g., Medpor) can provide good aesthetic outcomes, studies report higher complications including extrusion and infection when compared to rib reconstruction.[3,4]

3D printing may lessen the technical complexity of autologous implants and produce high-fidelity, biocompatible constructs similar to native tissues using tissue engineering. Some challenges with tissue engineering ear cartilage to date have been framework contraction/distortion, poor long-term outcomes, and high regulatory burden using complex in vitro methods out of the operating room.[5–8]

To address these limitations, we have developed a hybrid scaffold-based tissue engineering approach that also allows inclusion of point-of-care autologous cartilage tissue. We previously demonstrated that our auricular scaffolds promote chondrogenesis, as seeded chondrocytes induced chondrocyte proliferation in vitro.[9] Here, we

propose using bioscaffolds to promote chondrogenesis in clinically translatable settings that do not require an in vitro culture, a novel method that would have low regulatory burden, ease of performance, and capability to execute in a lower resource setting, such as global outreach initiatives.

MATERIALS AND METHODS

In Vivo Models

Scaffold development. To produce the unseeded scaffold, an external anatomic envelope was derived from computed tomography (CT) imaging of a 10-year-old male and three-dimensional (3D) printed in bioresorbable polycaprolactone (PCL) with orthogonally interconnected spherical pores with a mean pore diameter of 2 mm.[9,10] For cartilage-seeded scaffolds, scaffolds were printed with five 2.7-mm-diameter tissue inset wells at areas previously determined using nonlinear finite element analysis (FEA) to experience high effective strain leading to ulceration. All scaffolds were sterilized with ethylene oxide prior to experimentation as in prior clinical 3D printing work.[11]

Unseeded scaffold implantation. All animal surgery protocols were approved by the Institutional Animal Care and Use Committee at the University of Michigan (PRO00009569). Unseeded scaffolds were implanted into a subcutaneous pocket within the dorsum of five athymic rats (hereafter referred to as control group rats 1–5). Ketoprofen was administered during surgery to prevent postoperative inflammation. Incisions were closed with a subcuticular absorbable suture and covered with cyanoacrylate tissue adhesive (3M, St. Paul, MN). Following surgery, rats were given E-collars and had their nails trimmed regularly to prevent aggressive grooming and self-induced damage to the skin over the scaffolds.

Cartilage-seeded scaffold implantation. Porcine auricles were procured approximately 16 hours prior to operating, prepared with chlorhexidine and betadine administration, then briefly kept at 2°C. The day of operation, cartilage was dissected out from skin under sterile conditions leaving the overlying perichondrium. Next, 3.5-mm punch biopsies were procured and rinsed in sterile phosphate-buffered saline with 250 U/mL bacitracin and 2.50 μg/mL amphotericin B. Punch biopsies were inserted into each of the five predetermined tissue inset wells in the scaffold so that the tissue was slightly convex from the surface of the scaffold. Scaffolds were then implanted into the dorsum of five athymic rats (hereafter referred to as hybrid group rats 6–10) with perioperative administration of ketoprofen. Rats were treated with one dose of cefazolin at 25 mg/kg approximately 4 hours prior to scaffold implantation and amoxicillin/clavulanic acid at 25 mg/kg twice a day for 10 days following implantation.

Clinical evaluation. Rats were subject to a weekly photodocumentation protocol with measurement of the length, width, and height of their scaffolds. They were assessed twice weekly for scaffold extrusion, site infection, scaffold exposure/fracture, hematoma/seroma, or ulceration, with calculation of cross-sectional area of ulcers if present. Ulcers were classified according to the following system: 1) rat-induced if markings suggested self-induced injuries including scratch marks or bite marks; 2) scaffold-induced if ulceration was present overlying the scaffold but distinct from the suture line; 3) nonsurgical site, to include rat-induced or scaffold-induced injury outside the suture site; and 4) surgical site if ulceration was present at the suture site. Rats were sacrificed at 24 weeks with explantation of scaffolds unless otherwise stated. A two-tailed t test assuming equal variances was conducted between unseeded and cartilage-seeded scaffolds comparing the maximum

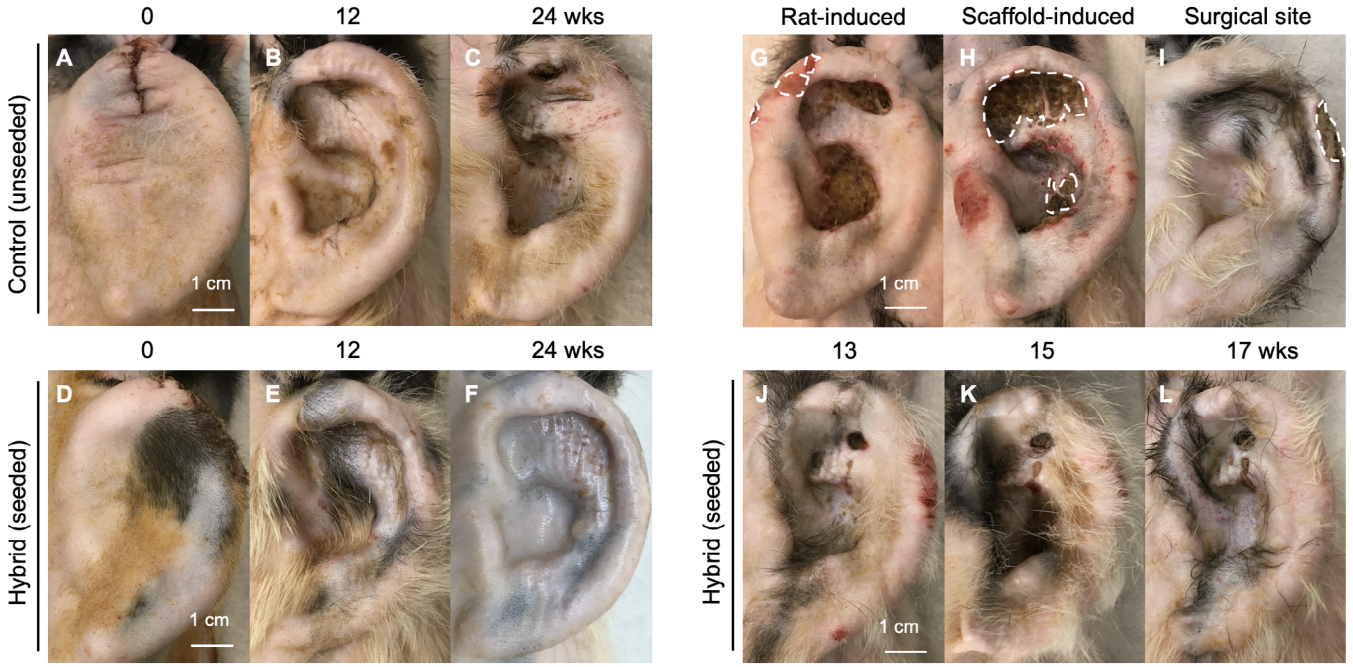

Fig. 1. Representation of scaffolds and/or ulcerations over time in vivo. Photodocumentation of a representative rat with unseeded scaffold (A) immediately following implantation, (B) 12 weeks after implantation, and (C) 24 weeks after implantation. (D) Photodocumentation of a representative rat with hybrid cartilage-seeded bioscaffold immediately after implantation, (E) 12 weeks after implantation, and (F) 24 weeks after implantation. Representative examples of (G) rat-induced, (H) scaffold-induced, and (I) surgical-site ulceration. Progression of nonsurgical and surgical site ulceration of representative rat with cartilage-seeded bioscaffold at (J) 13, (K) 15, and (L) 17 weeks after implantation, with demonstration of healing in lateral wounds.

cross-sectional areas for each ulcer classification, with $P < .05$ considered statistically significant.

Histological evaluation. Following explantation, three random samples of scaffold immediately surrounding punch biopsy insertion sites per rat were fixed in 4% formalin for 24 hours, embedded in paraffin, and processed using standard histologic procedures with a slice thickness of 10 μm. They were stained with hematoxylin and eosin (H&E) and Safranin O for cartilage growth assessment. Anti-pig Ki67 antibody (Neuromics, Edina, MN) was used to assess cellular proliferation in transplanted pig cartilage and anti-rat Ki67 (BD Pharmingen, San Diego, CA) for the surrounding tissue. Cleaved caspase 3 (Cell Signaling Technology, Danvers, MA) was applied for evaluation of cellular death in both pig and rat-related tissue. To assess vascularization, H&E slides were deidentified from their cohort (control vs. hybrid) and had four random images taken at 20× magnification (n = 12 per rat). Each image was assessed for number of vessels and the percent cross-sectional area of all blood vessels compared to overall image size (631 μm × 494 μm), where vasculature was defined by the presence of three distinct tunics (intima, media, and adventitia) with or without blood cells visible within the lumen of the vessel. Data were linked backed to the respective cohort, and unpaired two-tailed t tests assuming equal variances were conducted comparing number of vessels, average cumulative percent vessel area, and average percent vessel area per vessel, with $P < .05$ considered statistically significant.

Radiological evaluation. Following explantation, random samples of scaffold immediately surrounding punch biopsy insertion sites were placed in a 19-mm-diameter specimen holder and scanned using a microCT system (μCT100; Scanco Medical, Bassersdorf, Switzerland) with the following settings: voxel size 12 μm, 55 kVp, 109 μA, 0.5-mm AL filter, and integration time of 500 milliseconds. Scans were processed using Mimics (Materialise, Leuven, Belgium) to form 3D pictures.

Biomechanical evaluation. Nonlinear FEA of scaffolds was performed using FEBio (https://febio.org),[12] modeling skin,[13] and auricular cartilage[14] as nonlinear elastic materials undergoing large deformation with frictionless sliding contact conditions assumed between skin and ear scaffolds with and without biopsies.

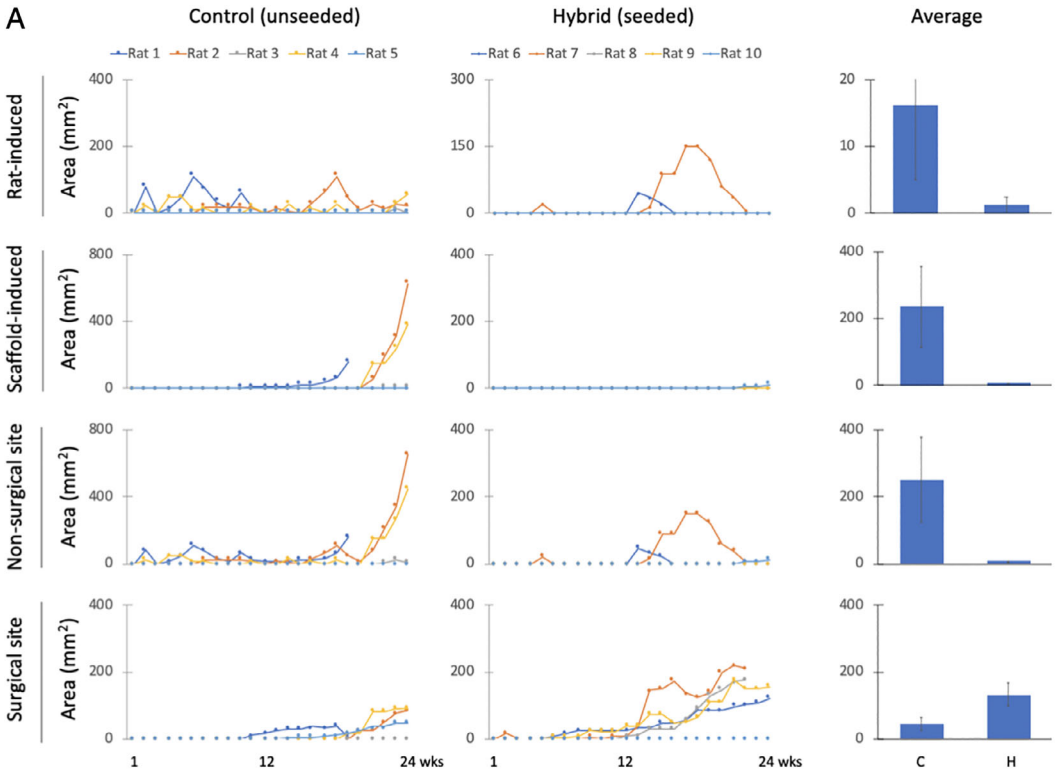

B

Ulceration	Control group Average	Control group SEM	Hybrid group Average	Hybrid group SEM	*P*-value
Rat-induced	135.0	80.4	3.2	2.1	0.140
Scaffold-induced	236.4	120.3	2.0	2.0	0.087
Non-surgical site	371.4	175.2	5.2	3.9	0.070
Surgical site	52.0	16.4	138.0	37.8	0.071

Fig. 2. Trended mitigation of a majority of soft-tissue ulceration mechanisms by hybrid approach. (A) Graphs representing cross-sectional area of ulcerations in control and hybrid groups according to type of ulceration (rat induced, scaffold induced, nonsurgical site, or surgical site) and average maximum cross-sectional area. Error bars represent standard error. (B) Average and standard error of the mean (SEM) of ulceration cross-sectional area in square millimeters in unseeded and cartilage-seeded scaffolds. *P* value was determined from two-tailed *t* test assuming equal variances.

RESULTS

Clinical Outcomes

Of rats with unseeded scaffolds, rats 2, 3, 4, and 5 made the 24-week target date. Rat 1 was sacrificed at 19 weeks after presenting with an enlarging skin rash and over 20% weight loss despite administration of empiric antibiotics and diet pills. Cultures yielded numerous *Streptococcus sciuri* and *Enterococcus faecalis* with varying susceptibilities, suggesting complicated wound infection. Of rats with cartilage-seeded scaffolds, rats 6, 9, and 10 made the 24-week target date. Rats 7 and 8 were sacrificed at 22 weeks because of worsening surgical site ulceration.

The progression of tissue overlaying the implants with time was monitored in the control (Fig. 1A–C) and hybrid groups (Fig. 1D–F). The average length, width, and height of scaffolds from both groups at 24 weeks was 62.6 ± 0.55 mm, 42.8 ± 0.45 mm, and 20.0 ± 0.00 mm

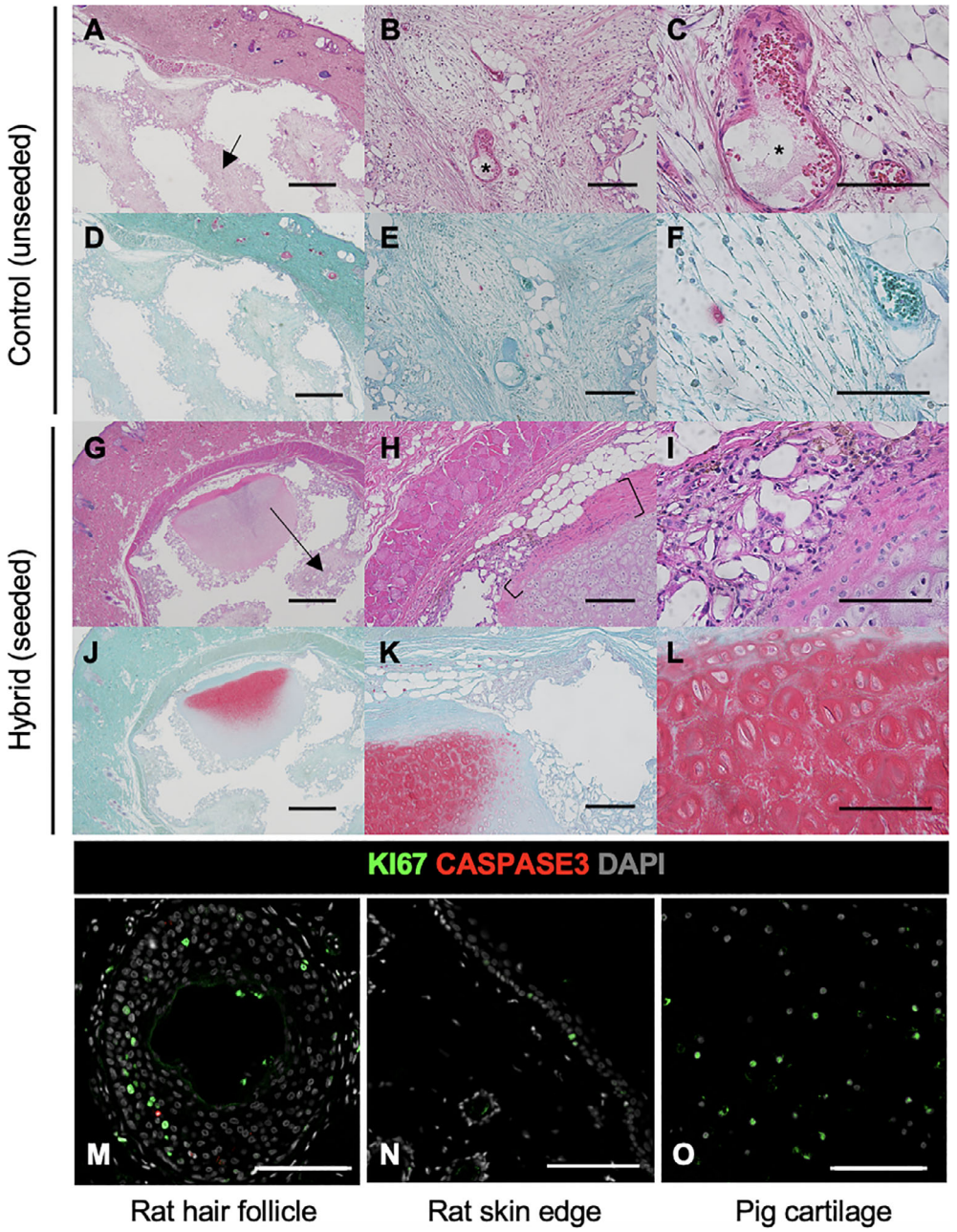

Fig. 3. Soft-tissue integration, angiogenesis, and maintenance of viable cartilage in the hybrid approach. Unseeded scaffold histology under hematoxylin and eosin (H&E) staining (A–C) and Safranin O staining (D–F). Cartilage-seeded scaffold histology with H&E staining (G–I) and Safranin O staining at (J–L). Scale bar represents 1,000 μm in panels A, D, G, and J; 200 μm in panels B, E, H, and K; and 100 μm in panels C, F, and I. Arrows point to soft tissue ingrowth. Asterisk represents vascularization. Brackets encompass viable perichondrium. Immunohistochemical staining for Ki67 (green), caspase-3 (red), and 4′,6-diamidino-2-phenylindole (DAPI) (grey) at different localizations in and/or surrounding the cartilage-seeded bioscaffold (M–O). Scale bar represents 100 μm.

respectively, indicating that the size of the bioscaffold was stable in vivo. By visual comparison with original scaffolds, there was no distortion of auricular subunit landmarks (superior and inferior crus of the antihelix, stem of the antihelix, triangular fossa, scaphoid fossa, conchal bowl, tragus, antitragus, intertragic notch).

Different ulceration types predominated across the groups. In the control group, 80% (4/5) had rat-induced ulceration (Fig. 1G). Scaffold-induced ulcerations (80% of cases) (Fig. 1H), non–surgical site ulcerations (80% of cases), and surgical site ulcerations (80% of cases) (Fig. 1I) were observed at high rates in the control group. However, the hybrid group only presented with rat-induced ulceration in 40% (2/5) of the cases. The formation of scaffold-induced ulceration (20% [1/5]) and non–surgical site ulceration was also lower (40% [2/5]), whereas the presence of surgical site ulceration (80% [4/5]) remained equal compared to control.

Next, we analyzed the temporal progression of cross-sectional areas for each ulceration classification. The majority of rat-induced ulcers in both the control and hybrid groups appeared and regressed within 2 to 9 weeks with minimal wound care (Fig. 1J–L). Interestingly, although there was a progressive worsening of surgical site ulcerations in 80% of the animals from both groups, we observed a smaller incidence and severity of scaffold-induced ulcers in the hybrid group compared to control. Meanwhile, different patterns of non–surgical site ulcerations were found between groups, as scaffold-induced ulcerations were predominantly seen in the control group, whereas the hybrid group had more rat-induced ulcerations (Fig. 2A). When averaging the cross-sectional ulcerations over the two groups (Fig. 2B), we observed that the control group demonstrated more rat-induced and scaffold-induced ulcerations compared to the hybrid group, albeit not in a statistically significant fashion. In contrast, ulcerations in the hybrid group were more frequently observed at the surgical sites.

Histological Outcomes

We evaluated the histology and cellular behavior of unseeded and seeded scaffolds via H&E, Safranin O, and Ki67/caspase 3 staining. In the control group, soft tissue infiltration into the periphery of the pores (arrow) was observed with moderate vascularization (Fig. 3A–C, asterisk). However, no cartilage (red) was present as outlined by Safranin O staining (Fig. 3D–F); we attribute scant positivity for Safranin O to staining of hair follicles.[15] H&E histology did not show concern for inflammatory infiltrates or signs of infection. In the hybrid group, we also observed robust soft tissue infiltration into the pore (Fig. 3G–I, arrow) with moderate vascularization and viable perichondrium overlaying the cartilage (Fig. 3H, brackets). Critically, we also saw maintenance of viable cartilage (red) within the transplanted punch biopsies (Fig. 3J–L). Immunohistochemistry revealed proliferating pig cells in rat skin overlying the scaffold, as seen in hair follicles, and at the edge of the skin (Fig. 3M, N) without porcine Ki67 antibody positivity outside of the punch biopsy. Interestingly, histology of porcine cartilage seeded in the scaffold at 24 weeks also demonstrated actively proliferating cells without major cell death (Fig. 3M–O).

Vascularization and blood vessel ingrowth were robust in both unseeded and hybrid seeded scaffolds. Comparable numbers of vessels per image were found on average between the control and hybrid groups (6.19 vs. 6.25, $P = .96$, Fig. 4A). Significantly larger cumulative percent vessel areas were found in the control rats versus hybrid rats (3.18% vs. 1.87%, $P < .05$) but no statistical significance was found after standardizing for vessel number (0.91%/vessel vs. 0.61%/vessel, $P = .07$, Fig. 4B).

Radiological Outcomes

Lastly, we performed microCT on porcine cartilage punch biopsies implanted into the scaffold (Fig. 5A, cartilaginous positions circled and correlated to the explanted ear). FEA models with and without biopsies (Fig. 5B, C) demonstrate amelioration of strain between ear scaffolds and skin. As expected, 3D model–constructed microCT imaging of hybrid scaffolds at the time of explantation demonstrated infiltration of soft tissue into the pores (Fig. 5D, E).

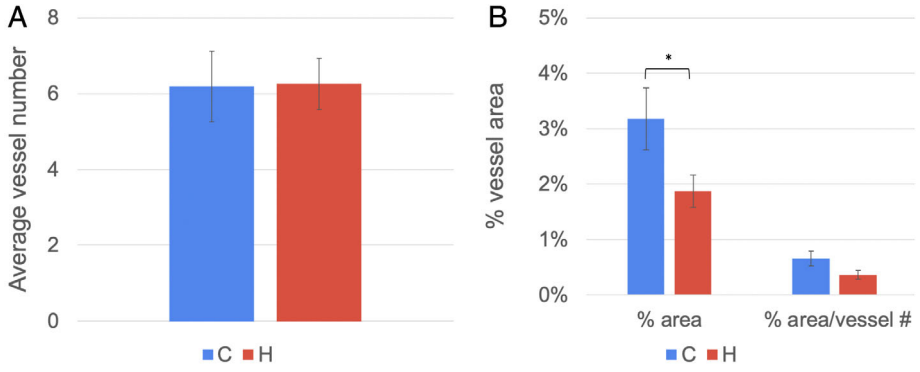

Fig. 4. Quantitative analysis of vascularization in control and hybrid rat scaffolds. (A) Average vessel number per image (311,714 μm^2). (B) Cumulative percent vessel area and percent vessel area normalized by vessel number per image. C = control group; H = hybrid group.

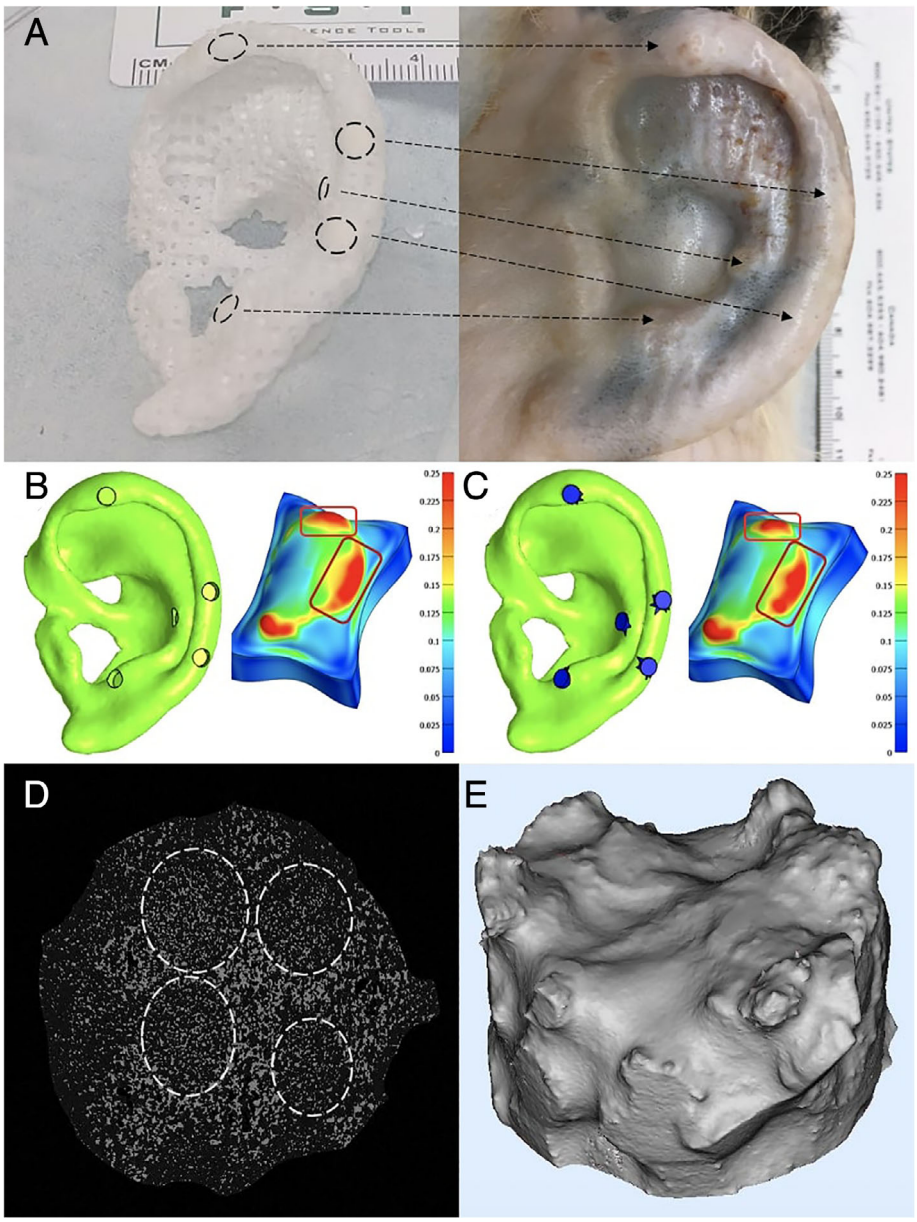

Fig. 5. Biomechanical modeling and micro–computed tomography (microCT) imaging of cartilage-seeded bioscaffolds. (A) A representative scaffold seeded with porcine auricular cartilage biopsies (circled) mapped to a hybrid scaffold. (B) Finite element analysis (FEA) model of polycaprolactone (PCL) scaffolds (green) without biopsy but containing insert holes and resulting strain in idealized skin pulled over the ear scaffold. (C) FEA model of PCL scaffolds with biopsy, resulting in reduced high-strain areas in idealized skin pulled over the ear scaffold. (D) MicroCT imaging of a cartilage-seeded scaffold with tissue infiltration circled. (E) Three-dimensional rendered model of a cartilage punch biopsy after explantation of the scaffold.

DISCUSSION

Several meaningful findings resulted from this study. First, implantation of biocompatible 3D-printed PCL scaffolds seeded with cartilaginous tissue was magnitudes less technically demanding than traditional autologous microtia reconstruction, more time efficient, and ultimately capable of sustaining viable cartilage. Grossly, 3D-printed auricles with and without cartilage inserts appeared structurally similar to human ears, and all scaffold measurements remained consistent. That no significant retraction or degradation of scaffolds was observed within the period of experimentation suggests resistance to myocontractile wound-healing forces and sustained longitudinal feasibility of such implants. Moreover, at the time of implantation, biopsies were intentionally larger than inset sites to allow securement through slight compression. Although inconspicuous in most cases, they were clearly visible in multiple scaffolds and found to be consistently intact on explantation without displacement; one punch biopsy may be seen prominently at the midstem of the helix in Figure 1F, for instance.

Critically, vascularization was identified by H&E staining in both unseeded and seeded scaffolds, implying that nonautologous tissue implants do not inhibit vessel formation within the timeframe of our experimentation. Although statistically greater cumulative percent vessel area was found in unseeded versus seeded scaffolds, comparable vessel number between the two cohorts and the difference in percent area was rendered not statistically significant on standardization by vessel number. These differences may be explained in multiple ways. Quantification of angiogenesis has inherent challenges based on how histology captures the blood vessels. We attempted to mitigate this by taking multiple samples per slide and multiple slides per position, but acknowledge that our measurement may be inaccurate and/or underestimated based on scoring from the H&E staining. Finally, although statistical differences were observed, they still arose only in the context of two cohorts of five rats each, and this study was not specifically powered to detect differences between the groups. Overall, vascularization was detected both grossly and histologically in each of the seeded and unseeded scaffolds, and we believe this level of vascularization is likely to improve overlying soft tissue quality when compared to the high-density nature of PPE.[16,17]

Regarding chondrogenesis, viable cartilage was confirmed by Safranin O in punch biopsy sites along with Safranin O–positive tissue on the periphery of the pores in the seeded scaffold. In addition to cartilage, viable perichondrium was observed on histology. Studies have previously established that chondrocyte progenitor cells are found within the perichondrium of adult auricular tissue.[18] With demonstration of perichondrial survival, we can envision coculturing perichondrium with multipotent cell populations—for example, adipose-derived stem cells—to evaluate its impact on differentiation and chondrogenic potential. Subjectively, we noted that the soft tissue overlying the scaffolds was thicker in tissue-seeded versus unseeded scaffolds, as seen in Figure 3A compared to Figure 3G. However, additional analysis is required to confirm these differences.

Distinct patterns of ulceration were noted between the unseeded and cartilage-seeded scaffolds. First, healing of rat-induced ulceration was seen across both conditions, consistent with the discovery of vascularization. Second, smaller rates of scaffold-induced ulceration approaching statistical significance were seen in the cartilage-seeded scaffolds. This suggests that inclusion of the cartilage tissue biopsies intended to offset the interface between overlying soft tissue, and that rigid scaffold was successful in ameliorating frictional strains, consistent with our FEA models in Figure 5B and C. Finally, it appears that a greater cross-sectional area of surgical site ulceration was present with the cartilage-seeded scaffolds compared to unseeded scaffolds, although this difference was not statistically significant. We hypothesize that even a slight increase in the volume of the offset may add small but meaningful amount of stress on the wound closure and that our closure technique utilizing a subcutaneous running Monocryl, which normally performs well in humans, might be more challenging in the postoperative care of animals. In the future, we could potentially address this complication by decreasing projection of the cartilage from the scaffold and balancing tension with a contralateral otoplasty.

There exist several key points that merit discussion. The first is that no statistically significant difference was observed between cartilage-seeded and unseeded scaffolds in any category of ulceration. This is likely due to limited sample size and the methods by which measurements were obtained. In the rat-induced ulceration category for example, it is possible that there are multiple occult signs that were not accounted for, including rubbing on the sides of the cage with subsequent scaffold displacement. Beyond statistical analysis, the exact relationship between Safranin O–positive tissue and chondrogenesis could not be determined with regard to the originating tissue. Specifically, one can imagine scenarios in which porcine cartilage induced a microenvironment whereby native circulating mesenchymal stem cells seeded around the punch biopsy were induced toward the chondrocytic lineage, or alternatively, where porcine mesenchymal stem cells were transplanted along with the auricular tissue and contributed to peripheral chondrogenesis. As such, additional immunohistochemistry will be essential for clarifying whether chondrocytes are present beyond the limits of the cartilage punch biopsy and from which tissue they arise.

Although the utility of 3D printing has grown dramatically in medicine at large, cartilage engineering in particular has benefited from its developments. Successful cartilage growth was shown by Cohen et al. in athymic rat and mouse models with implantation of bioscaffolds seeded with in vitro cultured chondrocytes and mesenchymal stem cells.[19] Kim et al. seeded 3D-printed auricular scaffolds with tonsil-derived mesenchymal stem cells, then implanted those scaffolds into mouse models with demonstration of collagen and vascularization after 12 weeks.[20] Additionally, Zhou et al. isolated auricular cartilage-derived chondrocytes from microtia patients, cultured them in a bioscaffold for 4 months, and implanted them back into the patients to observe successful outcomes after 2.5 years.[21] All of these concepts are promising, but unfortunately require a significant in vitro component with extensive culturing time that may not be readily translatable in all institutions. Furthermore, these cells cultured outside the operating room combined with scaffolds are a class III combination product that face significant regulatory expense and time to achieve Food and Drug Administration approval for clinical use including performing phase I and phase II clinical trials. Exclusively in vivo approaches have been tried too, with chondrogenesis obtained in bioscaffolds seeded with autologous diced cartilage and platelet-rich plasma in rabbit models.[22] However, even this required some processing after collecting tissue/serum, and a cystic-like reaction was induced around the scaffold at explantation at 4 months, indicating that improvements are still warranted. In comparison to these methods, our work has fewer technical requirements in combining point of care tissue engineering with 3D printing and do not require advanced technology, for example, bioprinting with cells

plus materials. As a result, this work has great potential in global outreach, where organizations and facilities may not have the same capacities as those within the United States.

CONCLUSION

We show a promising new technique for auricular reconstruction that is reproducible, relatively less technically complex, and most importantly, readily clinically translatable as it eliminates in vitro requirements and accompanying regulatory burden. One can imagine a situation in which a bioscaffold is customized and printed for a patient, seeded with autologous tissue, and implanted within the same day. With further iterations, we hope to expand this project to additional animal models, use autologous tissues, extend the period of observation after implantation, and ultimately translate toward human patients.

ACKNOWLEDGMENTS

The authors thank the Extracorporeal Circulation Research Laboratory and Dr. Hsun-Liang Chan of the Department of Periodontics and Oral Medicine for their donation of pig tissue, and Drs. Patrick Lester and Anna Skorupski of the Animal Care and Use Program for their assistance in animal care.

BIBLIOGRAPHY

1. Cubitt JJ, Chang LY, Liang D, Vandervord J, Marucci DD. Auricular reconstruction. *J Paediatr Child Health* 2019;55:512–517.
2. Olshinka A, Louis M, Truong TA. Autologous ear reconstruction. *Semin Plast Surg* 2017;31:146–151.
3. Cenzi R, Farina A, Zuccarino L, Carinci F. Clinical outcome of 285 Medpor grafts used for craniofacial reconstruction. *J Craniofac Surg* 2005;16: 526–530.
4. Constantine KK, Gilmore J, Lee K, Leach J Jr. Comparison of microtia reconstruction outcomes using rib cartilage vs porous polyethylene implant. *JAMA Facial Plast Surg* 2014;16:240–244.
5. Reiffel AJ, Kafka C, Hernandez KA, et al. High-fidelity tissue engineering of patient-specific auricles for reconstruction of pediatric microtia and other auricular deformities. *PLoS One* 2013;8:e56506.
6. Bichara DA, O'Sullivan NA, Pomerantseva I, et al. The tissue-engineered auricle: past, present, and future. *Tissue Eng Part B Rev* 2012;18:51–61.
7. Tack P, Victor J, Gemmel P, Annemans L. 3D-printing techniques in a medical setting: a systematic literature review. *Biomed Eng Online* 2016; 15:115.
8. Jung CS, Kim BK, Lee J, Min BH, Park SH. Development of printable natural cartilage matrix bioink for 3D printing of irregular tissue shape. *Tissue Eng Regen Med* 2018;15:155–162.
9. Zopf DA, Flanagan CL, Mitsak AG, Brennan JR, Hollister SJ. Pore architecture effects on chondrogenic potential of patient-specific 3-dimensionally printed porous tissue bioscaffolds for auricular tissue engineering. *Int J Pediatr Otorhinolaryngol* 2018;114:170–174.
10. Zopf DA, Mitsak AG, Flanagan CL, Wheeler M, Green GE, Holliser SJ. Computer aided-designed, 3-dimensionally printed porous tissue bioscaffolds for craniofacial soft tissue reconstruction. *Otolaryngol Head Neck Surg* 2015;152:57–62.
11. Zopf DA, Hollister SJ, Nelson ME, Ohye ERG, Green GE. Bioresporbable airway spint created with a three-dimensional printer. *N Engl J Med* 2013;368:2043–2045.
12. Maas SA, Ellis BJ, Ateshian GA, Weiss JA. FEBio: finite elements for biomechanics. *J Biomech Eng* 2012;134:011005.
13. Shergold OA, Fleck NA. Experimental investigation into the deep penetration of soft solids by sharp and blunt punches, with application to the piercing of skin. *J Biomech Eng* 2005;127:838–848.
14. Zopf DA, Flanagan CL, Nasser HB, et al. Biomechanical evaluation of human and porcine auricular cartilage. *Laryngoscope* 2015;125: E262–E268.
15. Safranin. Conduct Science website. Available at: https://conductscience.com/lab/safranin/. Accessed April 22, 2020.
16. Stephan S, Reinisch J. Auricular reconstruction using porous polyethylene implant technique. *Facial Plast Surg Clinics of North Am* 2018;26:69–85.
17. Schroeder MJ, Lloyd MS. Tissue engineering strategies for auricular reconstruction. *J Craniofac Surg* 2017;28:2007–2011.
18. Togo T, Utani A, Naitoh M, et al. Identification of cartilage progenitor cells in the adult ear perichondrium: utilization for cartilage reconstruction. *Lab Invest* 2006;86:445–457.
19. Cohen BP, Bernstein JL, Morrison KA, Spector JA, Bonassar LJ. Tissue engineering the human auricle by auricular chondrocyte-mesenchymal stem cell co-implantation. *PLoS One* 2018;13:e0202356.
20. Kim HY, Jung SY, Lee SJ, Lee HJ, Truong MD, Kim HS. Fabrication and characterization of 3D-printed elastic auricular scaffolds: a pilot study. *Laryngoscope* 2019;129:351–357.
21. Zhou G, Jiang H, Yin Z, et al. In vitro regeneration of patient-specific ear-shaped cartilage and its first clinical application for auricular reconstruction. *EBioMedicine* 2018;28:287–302.
22. Liao J, Chen Y, Chen J, et al. Auricle shaping using 3D printing and autologous diced cartilage. *Laryngoscope* 2019;129:2467–2474.